THE JOURNAL OF BIOLOGICAL CHEMISTRY VOL. 289, NO. 16, pp. 11242–11252, April 18, 2014

Computational and Experimental Studies on β-Sheet Breakers Targeting $A\beta_{1-40}$ Fibrils

Received for publication, November 22, 2013, and in revised form, February 3, 2014 Published, JBC Papers in Press, February 28, 2014, DOI 10.1074/jbc.M113.537472

Velia Minicozzi[‡1], Roberta Chiaraluce[§], Valerio Consalvi[§], Cesare Giordano[¶], Claudia Narcisi[‡], Pasqualina Punzi[‖], Giancarlo C. Rossi[‡], and Silvia Morante[‡]

From the [‡]Department of Physics, University of Rome Tor Vergata and Istituto Nazionale di Fisica Nucleare (INFN), Viadella Ricerca Scientifica 1, 00133 Roma, Italy and [§]Department of Biochemistry, [¶]Biomolecular Chemistry CNR Institute, and [‖]Department of Chemistry, Sapienza University of Rome, P. le Aldo Moro 5, 00185 Roma, Italy

Background: β-Amyloid aggregates are at the basis of Alzheimer disease development. Short synthetic peptides are seen to inhibit polymerization.
Results: Various synthetic peptides have been studied by MD simulations and tested experimentally.
Conclusion: Combined results indicate Ac-LPFFN-NH_2 as an effective lead compound able to slow down $A\beta_{1-40}$ aggregation.
Significance: Designing potential Aβ aggregation inhibitors will help fight Alzheimer disease.

In this work we present and compare the results of extensive molecular dynamics simulations of model systems comprising an $A\beta_{1-40}$ peptide in water in interaction with short peptides (β-sheet breakers) mimicking the 17–21 region of the $A\beta_{1-40}$ sequence. Various systems differing in the customized β-sheet breaker structure have been studied. Specifically we have considered three kinds of β-sheet breakers, namely Ac-LPFFD-NH_2 and two variants thereof, one obtained by substituting the acetyl group with the sulfonic amino acid taurine (Tau-LPFFD-NH_2) and a second novel one in which the aspartic acid is substituted by an asparagine (Ac-LPFFN-NH_2). Thioflavin T fluorescence, circular dichroism, and mass spectrometry experiments have been performed indicating that β-sheet breakers are able to inhibit *in vitro* fibril formation and prevent the β sheet folding of portions of the $A\beta_{1-40}$ peptide. We show that molecular dynamics simulations and far UV circular dichroism provide consistent evidence that the new Ac-LPFFN-NH_2 β-sheet breaker is more effective than the other two in stabilizing the native α-helix structure of $A\beta_{1-40}$. In agreement with these results thioflavin T fluorescence experiments confirm the higher efficiency in inhibiting $A\beta_{1-40}$ aggregation. Furthermore, mass spectrometry data and molecular dynamics simulations consistently identified the 17–21 $A\beta_{1-40}$ portion as the location of the interaction region between peptide and the Ac-LPFFN-NH_2 β-sheet breaker.

Alzheimer disease belongs to a class of pathologies, generically known as amyloidoses, whose common feature is the switching of endogenous proteins or peptides from their physiological soluble configuration to a pathological fibrillar insoluble state (1, 2). The main proteinaceous component of amyloid deposition, detected in Alzheimer disease patient brains, is the so-called amyloid β peptide (Aβ),[2] normally from 39 to 43 amino acids long, that is produced by the cleavage of the amyloid precursor protein (APP).

The Aβ self-association process that appears to be responsible for amyloidogenesis and highly toxic fibril formation is preceded by a conformational modification in which the peptide partially loses its random coil or α-helical native structure that is locally replaced by a β-sheet structure (3–5).

The observation that short synthetic peptides called β-sheet breaker peptides (BSBps) are able to establish a direct interaction with soluble oligomers or amyloid aggregates, destabilizing the amyloidogenic conformer and thus precluding amyloid polymerization (6), was at the origin of a significant scientific effort with the ultimate hope of arriving at the development of an effective pharmacological strategy (7, 8).

The main idea driving these investigations is that fibril formation could be strongly suppressed if the residues belonging to the hydrophobic central region of the $A\beta_{1-40}$ sequence could interact with short peptides (9). This line of research was actively pursued by the Soto and co-workers (10). These authors have studied the effect of Ac-LPFFD-NH_2 (also known in the literature as iAβ5p) on the Aβ aggregation process. The Ac-LPFFD-NH_2 (customized with N- and C-terminal protections) specifically differs from the 17–21 (LVFFA) $A\beta_{1-40}$ fragment by having valine and alanine residues substituted by a proline and an aspartic acid residue, respectively. iAβ5p has been shown to possess a number of promising properties like the ability of crossing the blood-brain barrier and inhibiting (and disassembling) the formation of amyloid fibrils *in vitro* as well as *in vivo*. It has also been shown to prevent Aβ neurotoxicity in cell culture by blocking amyloid deposition and inducing dissolution of preformed plaques in amyloidosis rat brain models (11–13).

Recently Giordano *et al.* (14, 15) reported new iAβ5p analogues with several chemical modifications introduced to improve BSBps activity and metabolic stability. In particular

[1] To whom correspondence should be addressed: Dept. of Physics, University of Rome Tor Vergata, Viadella Ricerca, Scientifica 1, 00133 Roma, Italy. Tel.: 39-0672594554; Fax: 39-062023507; E-mail: minicozzi@roma2.infn.it.

[2] The abbreviations used are: Aβ, amyloid β peptide; APP, amyloid precursor protein; BSBp, β-sheet breaker peptide; Tau, taurine; MD, molecular dynamics; ThT, thioflavin T; ESI-MS, electrospray ionization-MS; Fmoc, *N*-(9-fluorenyl)methoxycarbonyl; r.m.s.d., root mean square deviation.

the taurine customized Tau-LPFFD-NH_2 peptide turned out to better bind $A\beta_{1-40}$ and to be more resistant to proteolysis.

To gain some insight in the effectiveness of such chemical modifications, it is necessary to understand at an atomistic level the nature of the interaction between $A\beta_{1-40}$ and different types of BSBps. With the purpose of establishing what determines the BSBp-specific chemical activity, we performed extensive classical molecular dynamics (MD) simulations on model systems where $A\beta_{1-40}$ in water is in interaction with different BSBps, specifically Ac-LPFFD-NH_2, Tau-LPFFD-NH_2, and the newly proposed Ac-LPFFN-NH_2.

MD simulations represent a powerful tool in the study of many interesting biological systems as they provide a description of the system physicochemical properties in terms of microscopic degrees of freedom. In particular MD simulations (classical (16), density functional theory (DFT) (17, 18), quantum mechanical (19)) have been largely employed in the study of proteins with the purpose of investigating their folding properties and, more recently, in the emerging field of metalloproteins and protein-metal interactions (20, 21). In the case of the Aβ peptide, MD results have been employed not only to guide experiments but have also been instrumental in designing potential Aβ aggregation inhibitors (22).

A key strategic feature of this work was to combine theoretical information from MD simulations with experimental results coming from a number of complementary techniques, such as thioflavin T (ThT) fluorescence, far UV circular dichroism (CD), and electrospray ionization mass spectrometry (ESI-MS). From this comparison it emerges that, among the three different kinds of BSBps we have studied and simulated, Ac-LPFFN-NH_2 appears to be the most efficient BSBp in slowing down and possibly preventing $A\beta_{1-40}$ aggregation. We regard this conclusion as an important result that encourages the use of MD simulations as a valuable tool for selecting potential lead compounds against fibril formation.

MATERIALS AND METHODS

We start by discussing the computational methods employed to perform classical MD simulations of systems made by one $A\beta_{1-40}$ in water in interactions with different BSBps. In the next subsections we will describe the experimental techniques we have set up to check the results of the theoretical investigations.

Computational Methods

We have performed extensive classical MD simulations of four different model systems. Three of them are prepared by dissolving in water 1 $A\beta_{1-40}$ and 10 copies of the 3 different BSBps we have considered, namely Ac-LPFFD-NH_2 and two variants of it, one obtained by substituting the acetyl group with taurine (Tau-LPFFD-NH_2) and the second by substituting the aspartic acid with an asparagine (Ac-LPFFN-NH_2). For comparison, a fourth model system with $A\beta_{1-40}$ in water in the absence of BSBps is simulated. We list in Table 1 the detailed chemical composition of the four systems we have studied with the nicknames we will be using all along the paper.

The $A\beta_{1-40}$ configuration that is used as a starting point in all the simulations is taken from the NMR structure of Crescenzi *et al.* (Ref. 23; Protein Data Bank ID 1IYT). It displays 2 α-helix regions (residues from 8–25 and residues 28–38) linked by a turn region (residues 26–27).

TABLE 1
Simulated systems: nicknames (left column); simulated systems composition (right column)

System name	Composition
abeta	$A\beta_{1-40}$ + 3 Na^+ + water
lpffd	$A\beta_{1-40}$ + 10 Ac-LPFFD-NH_2 + 3 Na^+ + water
taulpffd	$A\beta_{1-40}$ + 10 Tau-LPFFD-NH_2 + 3 Na^+ + water
lpffn	$A\beta_{1-40}$ + 10 Ac-LPFFN-NH_2 + 3 Na^+ + water

In each one of the three systems, the 10 copies of BSBps are initially inserted in an all-*trans* configuration. Their position and orientation are randomly chosen but are kept the same in the three systems. The simulation box is filled with a number of water molecules so as to have an ~400 mM $A\beta_{1-40}$ concentration. An appropriate number of Na^+ counter-ions is also added to have globally neutral systems.

Classical MD simulations are performed using the GROMACS package (24–27) with the inclusion of the GROMOS53A6 force field (28). The non-standard taurine force field is computed by using the Automated Topology Builder and Repository (29) and implemented within the GROMOS53A6 force field. Simulations are performed at neutral pH[3] in the NpT-ensemble. The temperature is kept constant (and equal to 300 K) by using the v-rescale thermostat (30) with a 0.1-ps coupling time. Pressure is kept constant at 1 bar by using the Berendsen barostat (31) with a 1-ps coupling time and an isothermal compressibility of 4.5×10^{-5} bar^{-1}. The single point charge (SPC) model is used for water molecules. Periodic boundary conditions are imposed to the system, and the Particle Mesh Ewald algorithm is employed in dealing with the long-range Coulomb interactions (32). The MD integration time step is 2 fs. A non-bond pair list (with a 1.4-nm cutoff) is updated every 10 steps. For each system in the study we collected trajectories as long as 80 ns.

The simulation strategy we used, identical in all the four cases, is the following. First of all, each system was relaxed in a vacuum via a steepest descent minimization. Then, after the appropriate number of counter-ions and water molecules was added, the solvent was relaxed by a few steps (10 ps) of NVT MD at 200 K leaving the solute untouched. At this point the whole system, solute and solvent, was equilibrated as a whole for 50 ps in the NVT ensemble at 300 K, and the final 80-ns-long NpT MD simulation at 300 K was started. To eliminate from the analysis possible unphysical transients due to lack of equilibration, only the last 50 ns were employed to extract structural information on the simulated systems. The analysis of MD trajectories was carried out by using both standard GROMACS tools as well as some expressly designed homemade codes.

Experimental Methods

Peptide Synthesis—$A\beta_{1-40}$ was purchased from the PolyPeptide Laboratories France SAS. The $A\beta_{17-21}$ and $A\beta_{25-35}$

[3] By "neutral pH" we mean that the protonation state of the peptide is chosen so as to have N terminus, arginine, and lysine protonated and positively charged and the C terminus, glutamic, and aspartic acid deprotonated and negatively charged. This choice corresponds to the expected protonation state of free amino acids at neutral pH.

TABLE 2
***m/z* experimental and theoretical values of $A\beta_{17-21}$, $A\beta_{25-35}$, and BSBps**

Peptide fragments	Molecular formula	*m/z* for $[M+H]^+$	
		Theoretical	Observed
$A\beta_{17-21}$	$C_{32}H_{45}N_5O_6$	596.3448	596.3497
$A\beta_{25-35}$	$C_{45}H_{81}N_{13}O_{14}S$	1060.5824	1060.5815
Ac-LPFFD-NH_2	$C_{35}H_{46}N_6O_8$	679.3455	679.3429
Tau-LPFFD-NH_2	$C_{35}H_{49}N_7O_9S$	744.3391	744.3379
Ac-LPFFN-NH_2	$C_{35}H_{47}N_7O_7$	678.3615	678.3658

fragments are synthesized by conventional solid phase chemistry (33) starting from Fmoc-Ala- and Fmoc-Met-Wang resin (150- mmol scale, 250 mg), respectively. Ac-LPFFD-NH_2, Ac-LPFFN-NH_2, and Tau-LPFFD-NH_2 peptides are synthesized on Rink amide resin (65-mmol scale, 100 mg). Fmoc-amino acids-OH (Fmoc-AA-OH), diisopropylcarbodiimide (DIC), and hydroxybenzotriazole (HOBt) (3 eq, respectively) in *N*-methyl-2-pyrrolidinone are used for couplings. The Fmoc-taurylsulfonyl chloride, required for the preparation of the Tau-containing derivative, was prepared according to Liskamp and co-workers (34) and coupled to the resin-bound protected pentapeptide in dichloromethane in the presence of 4-methylmorpholine (7 eq). The coupling mixture was shaken overnight. After cleavage, the crude peptides were purified by reverse phase-HPLC on a Waters 600E liquid chromatography system by using a Waters Bondapac C-18 column (1.9 × 30 cm, 5 μm, 300 Å) for semi-preparative scale with elution at 8 ml/min by a linear gradient of 10–60% acetonitrile in 0.1% aqueous trifluoroacetic acid in 30 min. Peptide purity is >97% by analytical HPLC (Waters μ-Bondapack C-18 column, 0.39 × 30 cm, 5 μm, 300 Å). The peptides were characterized on a Q-TOF MICRO spectrometer (Micromass, now Waters, Manchester, UK) equipped with an ESI source, in the positive ion mode, and data were analyzed using the MassLynx software (Waters). In Table 2 we compared the theoretical expected numbers with the values of *m/z* for the $[M+H]^+$ molecular ions associated to the $A\beta_{17-21}$, $A\beta_{25-35}$, Ac-LPFFD-NH_2, Tau-LPFFD-NH_2, and Ac-LPFFN-NH_2 peptides.

ThT Binding Assay—$A\beta_{1-40}$ aggregation was studied using a ThT binding assay (35). ThT fluorescence intensity was followed continuously in a PerkinElmer Life Sciences LS 50 B spectrofluorimeter thermostated at 293 K with excitation and emission wavelengths set at 450 and 484 nm, respectively. Fluorescence changes were monitored in a 1-ml cuvette under continuous stirring at 484 nm every 6 s with 5-s integration times over at least 3000 min. 1 mM ThT stock solution in water was prepared, aliquoted, and stored at 253 K. Before each experiment, an aliquot of ThT stock solution was thawed at 277 K shielded from light. A solution of 16.0 μM lyophilized $A\beta_{1-40}$ in 20 mM Tris-HCl, pH 7.4 (1 ml final volume), alone or in the presence of a 12 M excess Ac-LPFFD-NH_2 or Ac-LPFFN-NH_2, was transferred to a 1-ml cuvette, and 10 μl of 1 mM ThT was added. Dead time for measurements of fluorescence changes did not exceed 12 s. In the absence of $A\beta_{1-40}$, intensity at 484 nm of ThT alone was identical to that measured in the presence of any of the tested BSBps and did not change over 3000 min (data not shown).

Far UV CD Spectroscopy—Far UV CD (190–250 nm) measurements were performed with a Jasco J-720 spectropolarimeter in a 0.1-cm path length quartz cuvette thermostated at 293 K. The results are expressed in terms of the mean residue ellipticity [Θ] assuming a mean residue weight of 110 daltons per amino acid residue. Ac-LPFFD-NH_2 or Ac-LPFFN-NH_2 were dissolved in ultra high quality water, lyophilized, and stored at 253 K. For far UV CD spectral measurements, each lyophilized compound was dissolved in ultra high quality water. Aliquots of lyophilized $A\beta_{1-40}$ were dissolved in 20 mM Tris-HCl, pH 7.4, at 16.0 μM final concentration in the absence or presence of a 12 M excess of BSBp, and the far UV CD spectral changes, occurring upon fibril formation, were monitored at 293 K at increasing times from 0 to 50 h. The far UV CD spectra of Ac-LPFFD-NH_2 or Ac-LPFFN-NH_2 monitored from 0 to 50 h did not show any change as a function of time. Far UV CD spectra of $A\beta_{1-40}$ in the presence or in the absence of BSBps were analyzed by singular value decomposition (36–38) using the MATLAB (MathWorks, South Natick, MA) software.

Mass Spectrometry—All the mass spectrometry experiments were performed on a Q-TOF MICRO spectrometer (Waters) equipped with an ESI source in the positive ion mode, adjusting the operating parameters as follows: rate of sample infusion into the mass spectrometer 20 μl/min, capillary voltage 2.8 kV, source temperature 353 K, source pressure 1.30 mbar, cone voltage 35 V, collision energy 10 eV. Full scan MS spectra were recorded in the *m/z* range between 800 and 2500, with 100 acquisitions per spectrum. Data were analyzed using the MassLynx software developed by Waters. $A\beta_{1-40}$ spectra were obtained from samples dissolved in water at a 50 μM final concentration and pH 3.5. After the binding equilibrium was established, methanol (20% v/v) was added to the mixture just before injection to obtain a stable electrospray signal. The final volume of the sample was 200 μl. As a reference, a sample containing only $A\beta_{1-40}$ was prepared. The spectra of the 17–21 and 25–35 fragments were also taken in the same conditions except that a neutral pH was used. To minimize statistical errors, each experiment was repeated at least three times under the same experimental conditions.

RESULTS AND DISCUSSION

Computational Results—To identify the specific $A\beta_{1-40}$-BSBps structural features arising in the different physicochemical situations we have studied, we have found it useful to look at the evolution with the MD simulation time of a number of geometrical indicators and chemical properties.

Configuration Distance Indicator—Detailed and direct information on the time evolution of the $A\beta_{1-40}$ configuration can be extracted from the study of the root mean square displacement, r.m.s.d., evolution defined by the formula

$$\text{r.m.s.d.}\ (t) = \left[\frac{1}{N}\sum_{i=1}^{N}\left|r_i(t) - r_i(t_0)\right|^2\right]^{1/2} \qquad \text{(Eq. 1)}$$

where *N* is the number of selected (see after) atoms of $A\beta_{1-40}$, whose displacement with respect to the initial ($t = t_0$) configuration we wish to compute. As a reference configuration we take the initial Protein Data Bank $A\beta_{1-40}$ peptide structure, where the peptide is in a fully α-helix secondary structure. The

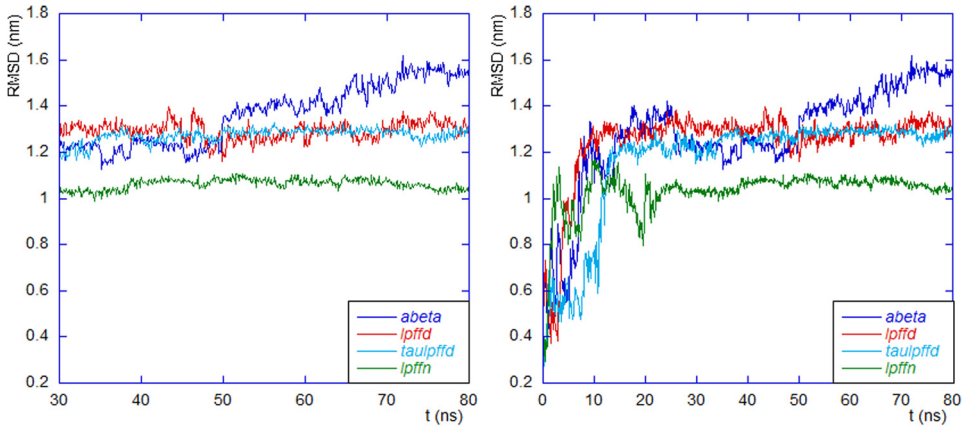

FIGURE 1. *Left panel*, the last 50 ns of the r.m.s.d. time evolution of all systems are shown. The Protein Data Bank structure is taken as reference configuration. The sum in Equation 1 is restricted to the $A\beta_{1-40}$ backbone atoms. *Right panel*, the full r.m.s.d. evolution where the initial time transient is also visible. Color code (see Table 1) is *blue* for Aβ; *red* for *lpffd*, *light blue* for *taulpffd*, and *green* for *lpffn*.

coordinates $\{r_i(t);\ i = 1, \ldots, N\}$ in Equation 1 were obtained after minimizing r.m.s.d.(t) over the rigid roto-translations of the current atomic configuration. r.m.s.d. was computed with the help of the g_rms (39) GROMACS tool.

In Fig. 1 the time behavior (from 30 ns on) of the r.m.s.d. of the $A\beta_{1-40}$ backbone atoms is displayed. For completeness, in the *right panel* of Fig. 1 we show the whole evolution where the transient phase is also visible.

We note that $A\beta_{1-40}$ in the *lpffn* system (*green curve*) shows the lowest values of r.m.s.d. This finding confirms that the $A\beta_{1-40}$ backbone undergoes the smallest structural change when in the presence of Ac-LPFFN-NH_2.

It is interesting to note that around 50 ns the r.m.s.d. of $A\beta_{1-40}$ in the *abeta* system suddenly jumps to a higher value that remains the highest till the end of our simulation. The r.m.s.d. jump occurs in coincidence with the appearance of a short β-sheet strand (see *panel a* of Fig. 2). Taken together, the two results suggest that the intramolecular β-sheet forms at the expense of a quite dramatic change of the global $A\beta_{1-40}$ configuration. Such a change was not observed when, as shown in *panels b* and *c* of Fig. 2, an intermolecular β-sheet formed between $A\beta_{1-40}$ and one of the BSBps in the *lpffd* and *taulpffd* systems or when an intermolecular β-sheet was formed between two BSBps, as happens in the case of the *lpffn* system (see *panel d* of Fig. 2). As will be confirmed under "Secondary Structure Analysis" below, this short β-sheet strand is located in front of the conserved 17–21 $A\beta_{1-40}\alpha$-helix segment.

Residue Mobility—The residue mobility, σ_R, of each amino acid along the sequence can be computed from the formula,

$$\sigma_R = \left[\frac{1}{T} \sum_i \frac{1}{N_R} \sum_i \left| r_j(t) - \langle r_j \rangle \right|^2 \right]^{1/2} \qquad \text{(Eq. 2)}$$

where T is the time length of the MD trajectory (here the last 50 ns), $\{r_j(t);\ i = 1, \ldots, N_R\}$ are the positions of the N_R atoms belonging to the residue R at time t, and $\langle r_j \rangle$ is the average position of each residue atom along the trajectory. The residue mobility was computed making use of the g_rmsf GROMACS tool.

In Fig. 3, σ_R was plotted against the residue position along $A\beta_{1-40}$ sequence. The color code used for the four panels is the same as in Fig. 1. It is pretty clear that the *abeta* system shows the highest σ_R values all along the sequence. In other words, one can say that $A\beta_{1-40}$ residue mobility is always reduced by the presence of any of the three BSBps. In this respect, again the most effective BSBp seems to be Ac-LPFFN-NH_2.

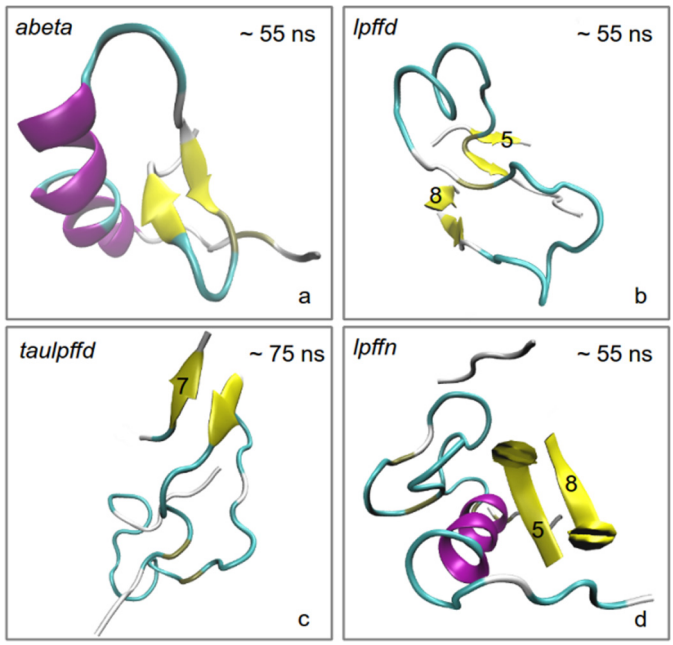

FIGURE 2. **For each one of the four simulated systems (see Table 1) a representative structural configuration (as defined by the g_cluster GROMACS tool) is drawn.** The time intervals where these structures were taken were selected among those within which a stable β-sheet structure was visible. These are 50–60 ns for systems *abeta* (*a*), *lpffd* (*b*), and *lpffn* (*d*) and 70–80 ns for the *taulpffd* system (*c*). The numbers in *panels b–d* identify the BSBps lying nearer to $A\beta_{1-40}$ (see also Fig. 4).

BSBp Docking—An important related structural question is where along the $A\beta_{1-40}$ sequence BSBps preferentially come in interaction with the peptide. In many existing numerical studies (40) simulations are started from configurations where BSBps, or other similar molecules, are located in the vicinity of preassigned peptide segments. In view of the strong biasing effect that such an a priori decision can have on simulation results, it is of the highest importance to examine the reliability of this strategy.

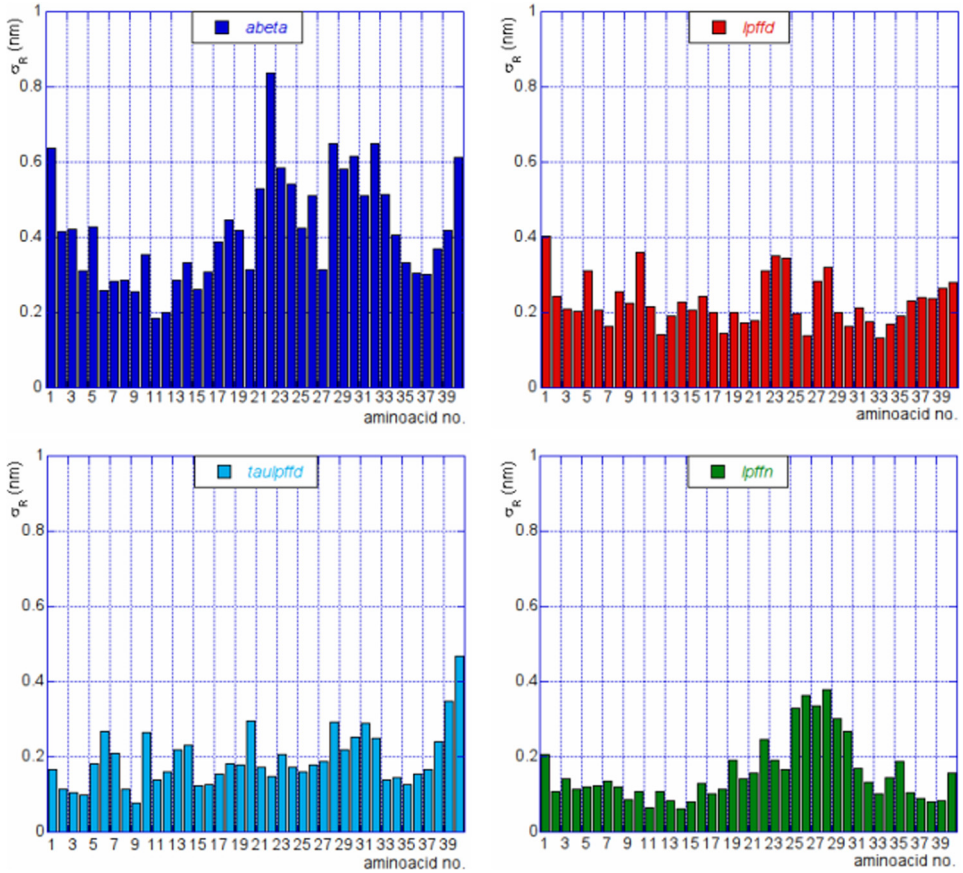

FIGURE 3. **Mobility of Aβ_{1-40} residues, σ_R (see Equation 2), is plotted against the residue number.** The color code is as in Fig. 1.

Thanks to the fact that we started our MD trajectories from configurations where BSBps are randomly distributed within the simulation box, we are able to check whether there are preferred docking regions for BSBps along Aβ_{1-40} sequence in an unbiased way.

To this end we have monitored the time evolution of the distance from Aβ_{1-40} of each of the 10 BSBps in the three-model systems, *lpffd*, *taulpffd*, and *lpffn*. We constructed plots (see Fig. 4) where for each 1 of the 10 BSBps a *dot* is drawn if its center of mass is within 8 Å from anyone of the Aβ_{1-40} backbone atoms. In these plots the whole 80 ns trajectory is displayed. From the 3 panels of Fig. 4 one concludes that, although the 10 BSBps in each model system start from the same position, those that come closer to the peptide are not always the same. Thus in the *lpffd* model system BSBps 5 and 8 come in contact with Aβ_{1-40}, and in the *taulpffd* system it is the BSBp 7 that after about 15 ns get stuck to the peptide, whereas in the case of *lpffn* the dynamics situation was more varied, but after a transient phase, the BSBps that finally come stably closer to the peptide are 1 5, and, for a long fraction of the simulation time, also 8 and 9.

Another important information is where the BSBp docking region along the peptide sequence is located. We can extract this information by monitoring the Aβ_{1-40} residues to which the BSBps in the various systems tend to come closer. In the six panels of Fig. 5 we display as a function of time the residues to which BSBps lie within 8 Å from the peptide. It is interesting to remark that, although the docking region is not always the same, in all the three model systems (*lpffd*, *taulpffd*, and *lpffn*) the region 25–35 (*i.e.* the Aβ_{1-40} most hydrophobic region) was always capable of attracting one of the BSBps. A reassuring conclusion from all the above analysis is that the initial BSBp configuration has little biasing effect on the long-time history of the system.

Secondary Structure Analysis—Using the standard protocol for the Definition of Secondary Structure of Proteins (DSSP) proposed by Kabsch and Sander (41), we plot in Fig. 6 the fraction of residues in different secondary structures (α-helix, coil, β-sheet, β-bridge, bend, turn, 5-helix, 3-helix) as a function of simulation time (the last 50 ns are shown).

The interesting pattern emerging from the comparison of the four plots needs some discussion. We start by noticing that in all cases Aβ_{1-40} has the tendency of loosing its initial (Protein Data Bank) α-helix structure (Fig. 6; *blue points*). This phenomenon, however, occurs at different degrees depending on the system. In the *lpffd* and *taulpffd* system the α-helix structure is completely absent (it was lost already in the first 30 ns of simulation; data not shown). In the case of the *abeta* system (peptide in the absence of BSBps) the α-helix remained confined to the 8–13 segment and was partially replaced (13–18 region) by the quite similar 5-helix structure (purple points).[4] Finally,

[4] This result may seem in contradiction with the simulation studies of Refs. 42 and 43, where it is claimed that the native α-helix structure of the peptide is completely lost in water. The reason for the discrepancy is most probably due to the different temperature at which simulations have been carried out, namely 300 K in our case and 360 K in Refs. 42 and 43.

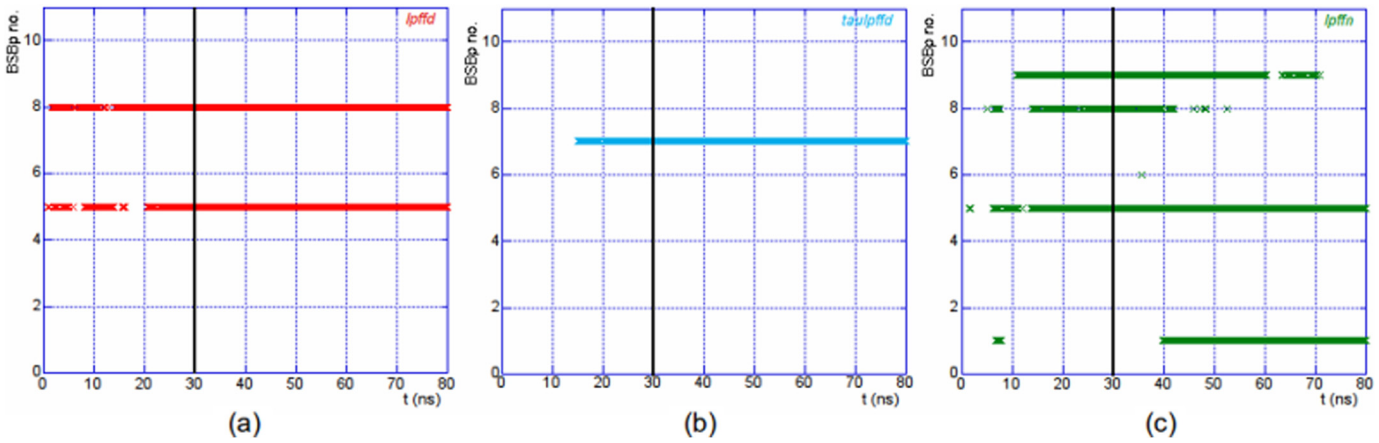

FIGURE 4. **BSBps lying within 8 Å from the $A\beta_{1-40}$ backbone are plotted as a function of simulation time.** The *black vertical line* marks the time $t = 30$ ns. The color code is as in Fig. 1.

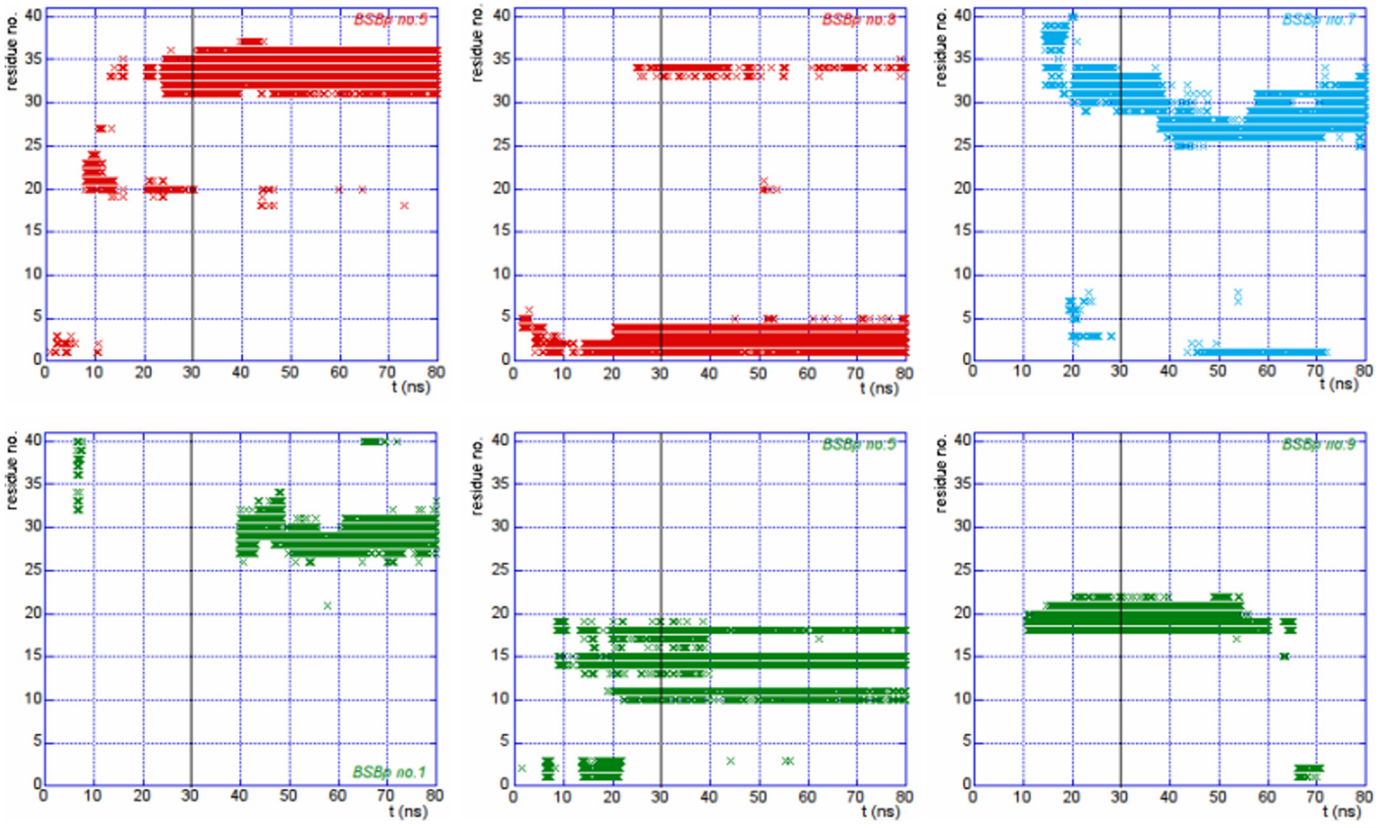

FIGURE 5. **$A\beta_{1-40}$ residues within 8 Å from the BSBps are displayed in Fig. 4, plotted as a function of simulation time.** In the panels we report data for the whole 80-ns MD trajectory. The *black vertical line* marks the time $t = 30$ ns. The color code is as in Fig. 1.

the longest sequence of residues (11–20 segment) that conserves an α-helix structure was found in the *lpffn* system, *i.e.* where $A\beta_{1-40}$ is in interaction with Ac-LPFFN-NH_2 (see *panel d* of Fig. 2). If the formation of (small) $A\beta_{1-40}$ aggregates is to be ascribed to the loss of the native α-helix structure, again the new Ac-LPFFN-NH_2BSBp appears to be in a better position than the other BSBps in suppressing peptide aggregation.

The Definition of Secondary Structure of Proteins analysis confirms the presence of short β-sheet strands (visible in Fig. 2, *panels a–c*) both in the case of $A\beta_{1-40}$ in the absence of BSBps in the time range between 52 and 58 ns and when the peptide was in interaction with Ac-LPFFD-NH_2, almost all along the trajectory.[5]

Because a β-sheet structure was supposed to favor aggregation, one might ask by which mechanism Ac-LPFFD-NH_2 is able to contrast peptide aggregation. We think that the answer can be found by looking at the overall structural arrangement of

[5] We did not see here the β-sheet structure visible at the end of the trajectory in *panel c* of Fig. 2 that refers to the case of $A\beta_{1-40}$ in the presence of Tau-LPFFD-NH_2. This difference was most probably due to the fact that the Definition of Secondary Structure of Proteins algorithm was slightly different from the one used by VMD that was employed to produce Figure 2.

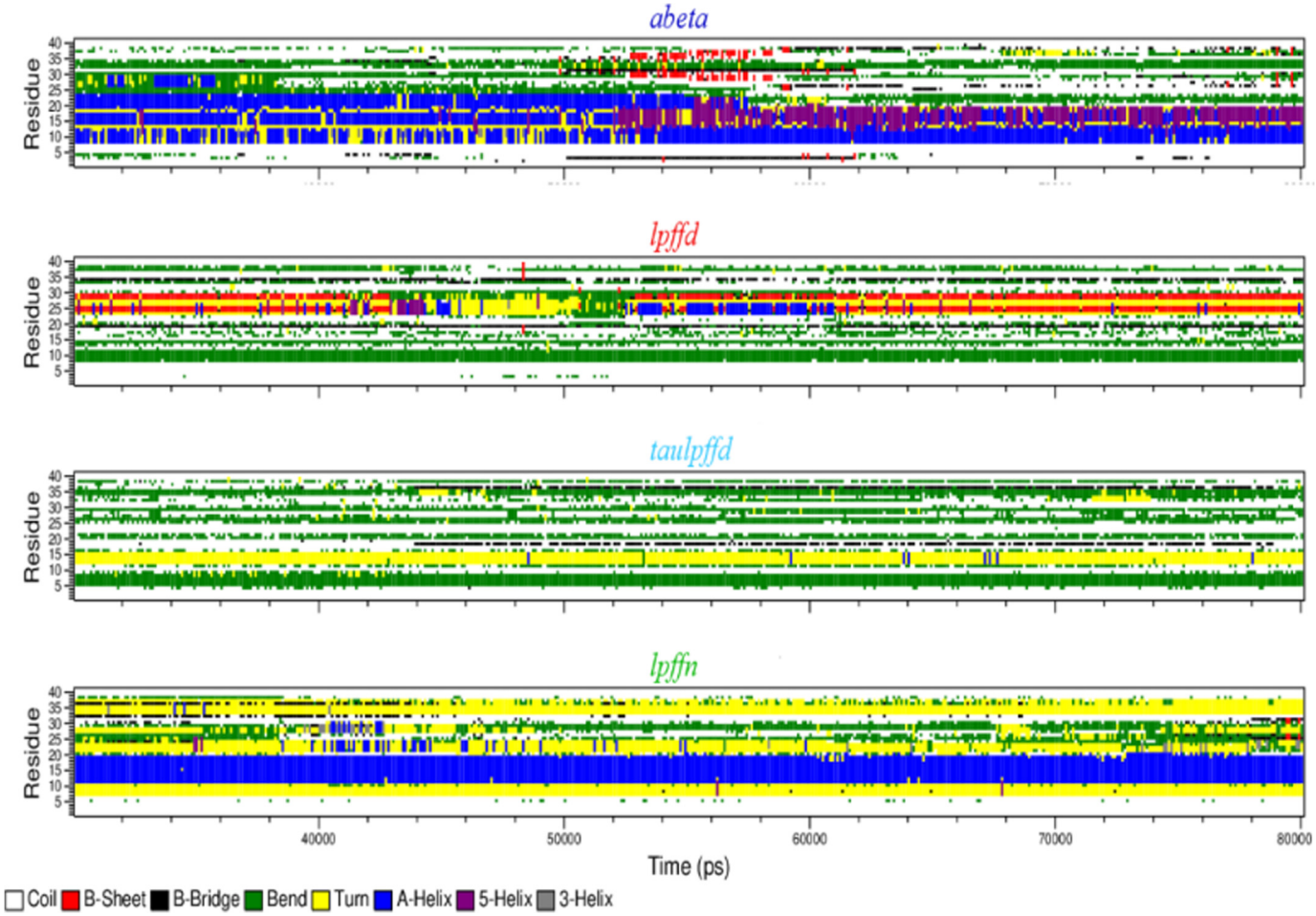

FIGURE 6. **$A\beta_{1-40}$ secondary structure time evolution (last 50 ns) in the four simulated systems.** In the *vertical axis* we plot the amino acid number along the $A\beta_{1-40}$ sequence. The color code of secondary structures is as follows: *white* for coil, *red* for β-sheet, *black* for β-bridge, *green* for bend, *yellow* for turn, *blue* for α-helix, *purple* for 5-helix, and *gray* for 3-helix structure.

the peptide with the BSBps that come close to it along the MD trajectory. Indeed, one notices that the β-sheet structure visible in the *lpffd* and *taulpffd* systems gets formed between an $A\beta_{1-40}$ segment and one of the BSBps (intermolecular β-sheet) and not within the peptide (intramolecular β-sheet).

The situation concerning the *lpffn* system was even more interesting. In fact, as shown in Fig. 2, *panel d*, now the β-sheet strand formed between two BSBps (*5* and *8*). The inter-BSBp β-sheet strand was located exactly in front of the conserved $A\beta_{1-40}$ α-helix region (residues 11–17), which in the *lowest panel* of Fig. 6 is represented by the blue strip extending all along the trajectory. We are led to the conclusion that the peptide α-helix stability in the 11–17 region is related to the formation of a β-sheet strand between two BSBps.

Our detailed simulations allow us to conclude that the first two tested BSBps (Ac-LPFFD-NH_2 and Tau-LPFFD-NH_2) act by somehow saturating (or hindering) the dangling bonds of a nascent β-sheet structure so that the latter are not available anymore for $A\beta_{1-40}$ aggregation. The third BSBp (Ac-LPFFN-NH_2), instead, in the very high BSBp:Aβ molar ratio (larger than 10:1) in which simulations and experiments (see next section) were carried out, act more by stabilizing the $A\beta_{1-40}$ α-helix structure (44, 45).

Experimental Results; ThT Binding Assay—The *in vitro* anti-aggregation activity of Ac-LPFFD-NH_2 or Ac-LPFFN-NH_2BSBps was monitored by measuring the changes in the relative fluorescence activity in the ThT binding assay. In Fig. 7 we show the results of the measurements of the relative fluorescence intensity at 484 nm as a function of time of three samples containing 16.0 μM $A\beta_{1-40}$ either alone or in the presence of 12 M excess of Ac-LPFFD-NH_2 or Ac-LPFFN-NH_2 BSBps.[6] Fluorescence measurements have been followed for a total time ranging from about 50 to 100 h.

The amplitude of ThT fluorescence (and thus the kinetics of $A\beta_{1-40}$ aggregation) is characterized by a time-dependent sigmoidal profile in which one can identify three phases, characterized by three different slopes: the lag phase, the growth exponential phase, and the final phase. ThT fluorescence amplitudes of all three samples increase with time and reach the same maximum. The length of the lag phase has been widely used in the literature as a diagnostic indicator of inhibition of $A\beta_{1-40}$ aggregation, as the longer the lag phase, the higher the BSBp inhibition activity. The main difference among the three sets of

[6] Experimental results on the Tau-LPFFD-NH_2 activity have been published in previous works (14,15).

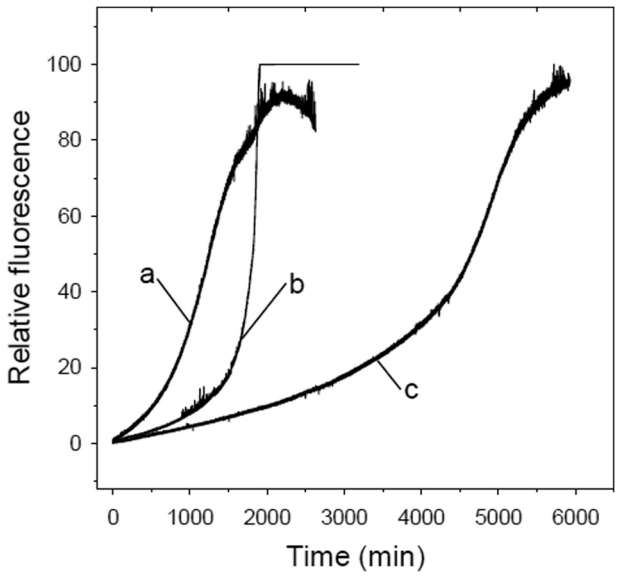

FIGURE 7. ***In vitro* activity of the Ac-LPFFD-NH_2 or Ac-LPFFN-NH_2 BSBps.** Fluorescence changes were monitored continuously at 393 K at 484 nm (450-nm excitation wavelength) in a 1-ml final volume containing 10 μM ThT, 16.0 μM $A\beta_{1-40}$ in 20 mM Tris-HCl, pH 7.4, alone (*a*) and in the presence of a 12 M excess of Ac-LPFFD-NH_2 (*b*) or Ac-LPFFN-NH_2 (*c*).

data is clearly in the lag phase. Indeed, when $A\beta_{1-40}$ is incubated with Ac-LPFFD-NH_2 or Ac-LPFFN-NH_2 the lag phase, namely the time needed to reach 20% of the maximal amplitude, passes from 600 min for the $A\beta_{1-40}$ in the absence of BSBps to 1000 min in the presence of Ac-LPFFD-NH_2 and up to 3000 min in the presence of Ac-LPFFN-NH_2.

Far UV CD Spectroscopy—Conformational studies on the synthetic lyophilized $A\beta_{1-40}$ in the absence or in the presence of BPBps were performed by monitoring the far UV CD spectral changes as a function of time, in parallel with the ThT binding assay and over the same time extent. Typically, $A\beta_{1-40}$ alone displayed the far UV CD spectral changes reported in Fig. 8, *panel A*.

The spectral changes of $A\beta_{1-40}$ in the absence of BSBps monitored over 50 h can be ascribed to an overall decrease of the negative molar ellipticity at around 198 nm, typical of turns-containing structure regions (46), accompanied by an increase of the negative molar ellipticity at around 215 nm, characteristic of β-sheet structure.

Two main spectral components are identified by singular value decomposition of the far UV CD spectra of $A\beta_{1-40}$ alone monitored over 50 h. The decrease of the negative molar ellipticity at around 198 nm (Fig. 8, *panel B*) can be mainly referred to the disappearance of turns-containing structure; the appearance of a β-sheet structure is revealed by the increase of the negative molar ellipticity at 215 nm and of the positive ellipticity at around 195 nm of the second spectral component (Fig. 8, *panel C*).

The *in vitro* inhibitory activity of Ac-LPFFD-NH_2 and Ac-LPFFN-NH_2 was tested by monitoring their efficacy in preventing and/or interfering with the $A\beta_{1-40}$ secondary structure conformational transition that is considered to precede the formation of fibrils and visible aggregates. The far UV CD spectra of $A\beta_{1-40}$ in the presence of Ac-LPFFD-NH_2 and Ac-LPFFN-NH_2BSBps were monitored from time 0 to about 3500 min and from time 0 to about 6800 min, respectively. The spectra have been analyzed by singular value decomposition, revealing two main spectral components centered at around 198 and 215 nm, respectively, similarly to what was observed in the case of the $A\beta_{1-40}$ alone. The changes at 198 nm and 215 nm visible in the first (*panel D* of Fig. 8) and the second (*panel E* of Fig. 8) spectral component were significantly reduced in amplitude in the presence of both BSBps.

A plot of the changes of molar ellipticity at 198 nm of the first spectral component of $A\beta_{1-40}$ alone as a function of time shows a sigmoidal profile with a jump of about 1.2×10^4 deg·cm^2·dmol^{-1} (see Fig. 8, *panel D*). In the presence of Ac-LPFFD-NH_2 or Ac-LPFFN-NH_2, the amplitude of the jump at 198 nm was significantly reduced with respect to that observed for $A\beta_{1-40}$ alone (see Fig. 8, *panel D*). As for the changes at 215 nm of the second spectral component in the presence of Ac-LPFFD-NH_2 or Ac-LPFFN-NH_2, they appeared to be negligible in comparison with those observed in $A\beta_{1-40}$ alone (Fig. 8, *panel E*). These results suggest that the interaction between $A\beta_{1-40}$ and Ac-LPFFD-NH_2 or Ac-LPFFN-NH_2 reduces the peptide conformational transition propensity.

When either Ac-LPFFD-NH_2 or Ac-LPFFN-NH_2 was present, there was an apparent discrepancy between ThT binding assay and far UV CD changes as a function of time (Fig. 8, *panels D* and *E*, *full triangles* and *full squares* stand for $A\beta_{1-40}$ in the presence of Ac-LPFFD-NH_2 and of Ac-LPFFN-NH_2, respectively). However, such results should be interpreted with caution at the high molar ratio ($A\beta_{1-40}$:BSBp = 1:12) at which experiments have been performed, as BSBps alone give far UV CD contribution in the same spectral range as $A\beta_{1-40}$ alone. The conformational changes of the BSBps in the presence of $A\beta_{1-40}$ are not known; thus the spectral changes of the samples simultaneously containing $A\beta_{1-40}$ and (a high concentration of) BSBps may be due to changes in $A\beta_{1-40}$ and/or BSBp. Results in this direction were reported in Laczkó *et al.* (47). In addition, it has been proposed (44, 45) that different pathways may lead to fibril formation and in the presence of certain inhibitors fibrillization may occur even in the absence of oligomerization/aggregation. Thus, the two processes may well proceed independently.

Mass Spectrometry—With the main purpose of identifying the site(s) where the interaction between Aβ and BSBps takes place and thus verifying MD simulations results, ESI-MS (48) was employed to directly detect Aβ-BSBp non-covalent complexes. The ESI-MS technique is a powerful diagnostic tool, as it is not only able to detect the existence of such complexes, but it also provides information on a number of interesting details about the BSBp $A\beta_{1-40}$ interaction. Because bound complexes can be transferred into the gas phase without the breaking of non-covalent bonds, the ESI MS technique allowed us to determine the location of the binding site(s), providing a measure of association ratio and interaction strength.

The mass spectrum of $A\beta_{1-40}$ in acetate buffer (1.0 mM with 0.5% acetic acid) at a 50 μM final concentration and pH 3.5 (data not shown) shows the typical peaks (49) at m/z = 866.6 (+5), 1083.1 (+4), 1443.8 (+3), and 2166.0 (+2) corresponding to the molecule with the ionization charges indicated in parentheses.

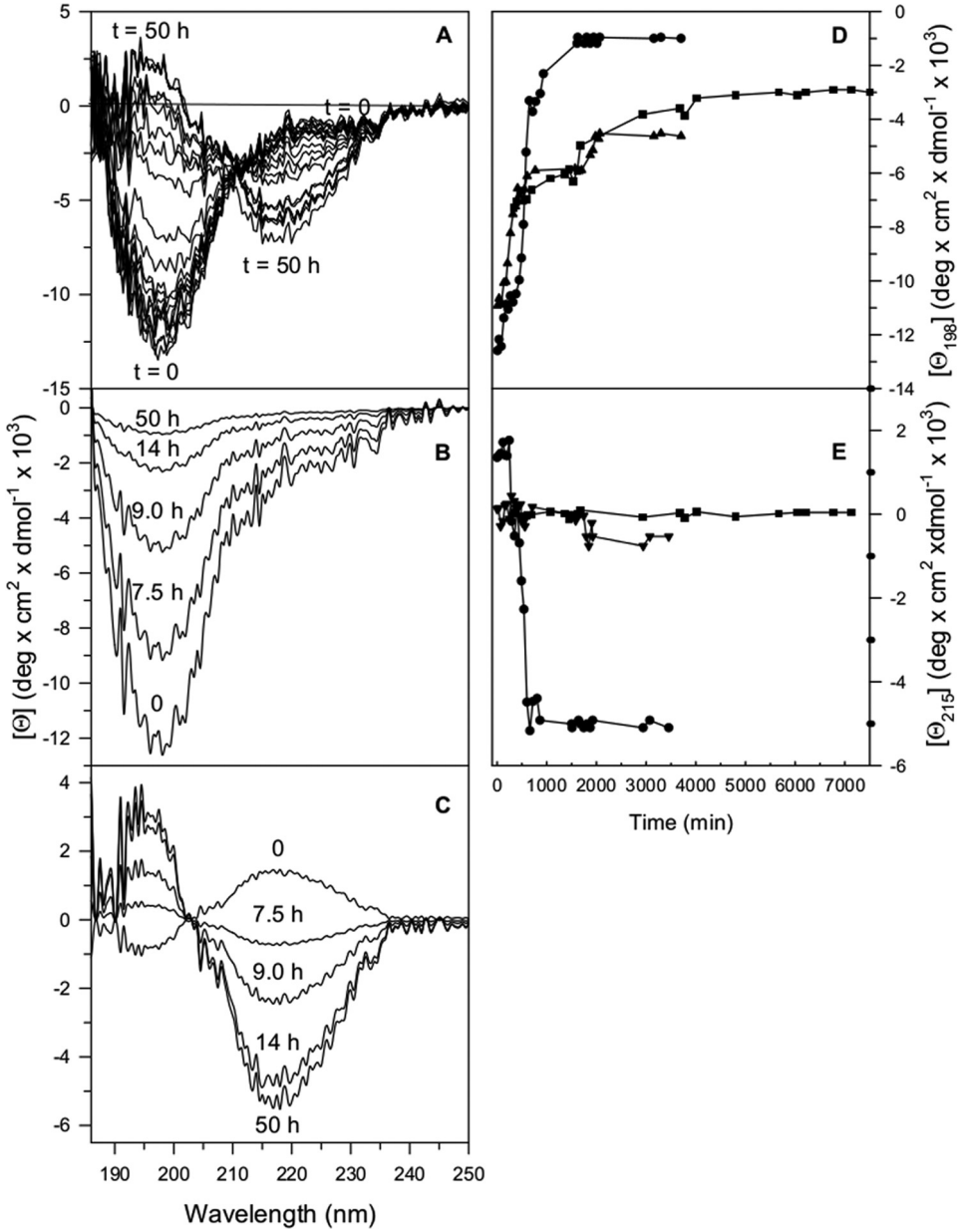

FIGURE 8. Far UV CD spectra of 16.0 μM Aβ_{1-40} in 20 mM Tris-HCl, pH 7.4, at 293 K is plotted as a function of time in the interval from 0 to 50 h (*A*). The first (*B*) and the second (*C*) spectral components of the far UV CD spectra of 16.0 μM Aβ_{1-40} in 20 mM Tris-HCl, pH 7.4, at 293 K are identified by singular value decomposition and plotted as a function of time in the interval from 0 to 50 h. The effect of BSBps on the far UV CD changes of Aβ_{1-40} is monitored at 198 and 215 nm. The changes at 198 nm (*D*) and at 215 nm (*E*) of the first and second spectral component, respectively, of 16 μM Aβ_{1-40} dissolved in 20 mM Tris-HCl, pH 7.4, are followed in the absence (*full dots*) and presence of a 12 M excess of Ac-LPFFD-NH_2 (*full triangles*) from 0 to 3500 min and of Ac-LPFFN-NH_2 (*full squares*) from 0 to 6800 min.

TABLE 3

Incubated BSBp (first column), K_1, K_2, and K_3 constants for equations 3, 4, and 5 (second, third, and fourth column), percentage of bound Aβ_{25-35} (fifth column), and fraction percentage of bound Aβ_{25-35} in equations 3, 4, and 5

BSBp	K_1	K_2	K_3	Bound Aβ_{25-35}	%
	M^{-1}	M^{-1}	M^{-1}	%	
Ac-LPFFD-NH_2	$3.92 \cdot 10^{-7}$	$4.34 \cdot 10^{-7}$	$1.55 \cdot 10^{-6}$	3.44	82/9/9
Tau-LPFFD-NH_2	$0.80 \cdot 10^{-7}$	$6.57 \cdot 10^{-7}$	$5.03 \cdot 10^{-7}$	2.80	77/14/9
Ac-LPFFN-NH_2	$1.55 \cdot 10^{-7}$	$3.68 \cdot 10^{-7}$	$1.66 \cdot 10^{-6}$	6.29	65/7/28

These numbers are consistent with a 4330.0-Da molecular mass. At neutral pH the mass spectrum shows, instead, the bell-shaped behavior typical of a polymerized amyloid from which no useful conclusions about the interaction properties of BSBp-Aβ_{1-40} complexes can be drawn.

After the addition of Ac-LPFFD-NH_2 to freshly prepared Aβ_{1-40} solution in equimolar ratio (both prepared in acetate buffer at pH 3.5), the mass spectrum displays, besides the previously mentioned Aβ_{1-40} peaks, new ion signals corresponding to the multiply charged Aβ-BSBp states (1:1 association

TABLE 4
Incubated BSBp (first column), K_1, K_2, and K_3 constants for equations 3, 4, and 5 (second, third, and fourth column), percentage of bound $A\beta_{17-21}$ (fifth column), and fraction percentage of bound $A\beta_{17-21}$ in equations 3, 4, and 5

BSBp	K_1	K_2	K_3	Bound $A\beta_{17-21}$	%
	M^{-1}	M^{-1}	M^{-1}	%	
Ac-LPFFD-NH_2	$4.62 \cdot 10^{-7}$	$6.07 \cdot 10^{-7}$	$1.65 \cdot 10^{-6}$	6.31	75/13/12
Tau-LPFFD-NH_2	$3.97 \cdot 10^{-7}$	$1.66 \cdot 10^{-7}$	$2.25 \cdot 10^{-7}$	7.49	91/5/4
Ac-LPFFN-NH_2	$9.20 \cdot 10^{-7}$	$3.07 \cdot 10^{-7}$	$4.69 \cdot 10^{-7}$	21.66	84/7/9

ratio) with charge +4 and +3 as well as peaks that can be attributed to multiply charged $(A\beta)_2$-BSBp states (2:1 association ratio) with charges +5, +6, and +7 (data not shown).

On the basis of these findings and with the aim of identifying which region of the $A\beta_{1-40}$ interacts with the ligand, we have studied the non-covalent interactions of Ac-LPFFD-NH_2 and of its two derivatives, Ac-LPFFN-NH_2 and Tau-LPFFD-NH_2, with the two peptide fragments, $A\beta_{25-35}$ and $A\beta_{17-21}$.

In Tables 3 and Table 4, the K_1, K_2, and K_3 constants refer to the three association reactions, respectively,

$$A\beta_{a\text{-}b} + BSBp_j \rightleftharpoons A\beta_{a\text{-}b} - BSBp_j \quad \text{(Eq. 3)}$$

$$A\beta_{a\text{-}b} - BSBp_j + A\beta_{a\text{-}b} \rightleftharpoons (A\beta_{a\text{-}b})_2 - BSBp_j \quad \text{(Eq. 4)}$$

$$A\beta_{a\text{-}b} - BSBp_j + BSBp_j \rightleftharpoons A\beta_{a\text{-}b} - (BSBp_j)_2 \quad \text{(Eq. 5)}$$

where *a-b* stands for the 25–35 (Table 3) or 17–21 (Table 4) fragment, and $BSBp_{j,j} = 1, 2$, and 3, are the three BSBps considered in this paper. The percentage of bound amyloid, given in the fifth column of the Tables 3 and 4, was computed as the ratio of the concentration of (single or pairs of) $A\beta_{a\text{-}b}$ fragments, bound with one or two BSBps with respect to the total $A\beta_{a\text{-}b}$ concentration. In the last column the fractions of bound $A\beta_{a\text{-}b}$ in reactions 3, 4, and 5 are reported.

From Tables 3 and 4 we see that the ESI-MS analysis exhibits an interesting distribution of multiply charged ions of $A\beta_{17-21}$ and $A\beta_{25-35}$ fragments and their complexes with BSBps in various stoichiometric combinations. In particular, the intensity of the observed peaks, corresponding to the various complexes formed by Aβ fragments bound to BSBps (data not shown), indicate that Ac-LPFFN-NH_2 binds more strongly than Ac-LPFFD-NH_2 and Tau-LPFFD-NH_2. In addition, Ac-LPFFN-NH_2 is seen to bind preferentially to the $A\beta_{17-21}$ fragment. All these experimental findings nicely confirm the MD simulations results we have previously presented.

Conclusions—MD simulation results show that essentially all the tested BSBps have the ability of reducing $A\beta_{1-40}$ residues mobility, with Ac-LPFFN-NH_2 as the most effective BSBp in this respect. A possible explanation for this feature is the following. In all the simulated systems one notices that, after the initial transient, some of the BSBps tend to approach the hydrophobic 25–35 region of $A\beta_{1-40}$, but the newly considered Ac-LPFFN-NH_2BSBp is also able to interact with the key hydrophobic 17–21 region. This significantly helps in preserving the native $A\beta_{1-40}$ α-helix secondary structure as it is confirmed by the persistency of the α-helix secondary structure throughout the whole MD simulation, visible in the 11–20 region of the *lpffn* system (see the *bottom panel* of Fig. 6).

Stimulated by the above MD results, we performed the same kind of experiments that were previously carried out on Ac-LPFFD-NH_2 and Tau-LPFFD-NH_2 in Giordano *et al.* (14,15) on Ac-LPFFD-NH_2 and on the new Ac-LPFFN-NH_2BSBp. As detailed under "*Experimental Results*," one finds that in the presence of Ac-LPFFN-NH_2 the formation of $A\beta_{1-40}$ fibrils was significantly delayed as indicated by the lag phase increase in ThT fluorescence experiments. Moreover, far UV CD measurements show that Ac-LPFFN-NH_2 stabilizes the $A\beta_{1-40}$ secondary structure, thus reducing the peptide β-sheet formation propensity. This stability may be considered the basis of the slowing-down of $A\beta_{1-40}$ aggregation indicated by ThT fluorescence experiments. Finally ESI-MS data clearly demonstrate that Ac-LPFFN-NH_2 preferentially interacts with the 17–21 hydrophobic $A\beta_{1-40}$ region.

All the collected experimental results are in very good agreement with MD simulations. In particular, MD simulations show that Ac-LPFFN-NH_2 binds via H-bonds to the 17–21 segment of $A\beta_{1-40}$ (consistently with what is suggested by ESI-MS data), precisely within the region where the native $A\beta_{1-40}$ α-helix secondary structure appears to survive solvation. We regard the overall consistency between experimental evidence and MD simulation results as a fairly strong indication that Ac-LPFFN-NH_2 can be an effective lead compound in preventing and/or destabilizing $A\beta_{1-40}$ aggregation.

Acknowledgment—We thank the AuroraScience project (funded by PAT and INFN) for allocating the computing resources for this project.

REFERENCES

1. Prusiner, S. B. (2001) Shattuck lecture. Neurodegenerative diseases and prions. *N. Engl. J. Med.* **344,** 1516–1526
2. Pepys, M. B. (2001) Pathogenesis, diagnosis, and treatment of systemic amyloidosis. *Philos. Trans. R. Soc. Lond. B. Biol. Sci.* **356,** 203–210
3. Serpell, L. (2000) Alzheimer's amyloid fibrils. Structure and assembly. *Biochim. Biophys. Acta* **1502,** 16–30
4. Soto, C., Castaño, E. M., Frangione, B., and Inestrosa, N. C. (1995) The α-helical to β-strand transition in the amino-terminal fragment of the amyloid β-peptide modulates amyloid formation. *J. Biol. Chem.* **270,** 3063–3067
5. Tomaselli, S., Esposito, V., Vangone, P., van Nuland, N. A., Bonvin, A. M., Guerrini, R., Tancredi, T., Temussi, P. A., and Picone, D. (2006) The α-to-β conformational transition of Alzheimer's Aβ-(1–42) peptide in aqueous media is reversible. A step by step conformational analysis suggests the location of β conformation seeding. *Chembiochem* **7,** 257–267
6. Soto, C. (1999) Plaque busters. Strategies to inhibit amyloid formation in Alzheimer's disease. *Mol. Med. Today* **5,** 343–350
7. Ghanta, J., Shen, C. L., Kiessling, L. L., and Murphy, R. M. (1996) A strategy for designing inhibitors of β-amyloid toxicity. *J. Biol. Chem.* **271,** 29525–29528
8. Gordon, D. J., and Meredith, S. C. (2003) Probing the role of backbone hydrogen bonding in β-amyloid fibrils with inhibitor peptides containing ester bonds at alternate positions. *Biochemistry* **42,** 475–485
9. Hilbich, C., Kisters-Woike, B., Reed, J., Masters, C. L., and Beyreuther K.

(1992) Substitutions of hydrophobic amino acids reduce the amyloidogenicity of Alzheimer's disease β A4 peptides. *J. Mol. Biol.* **228,** 460–473
10. Adessi, C., Frossard, M. J., Boissard, C., Fraga, S., Bieler, S., Ruckle, T., Vilbois, F., Robinson, S. M., Mutter, M., Banks, W. A., and Soto, C. (2003) Pharmacological profiles of peptide drug candidates for the treatment of Alzheimer's disease. *J. Biol. Chem.* **278,** 13905–13911
11. Soto, C., Kindy, M. S., Baumann, M., and Frangione B. (1996) Inhibition of Alzheimer's amyloidosis by peptides that prevent β-sheet conformation. *Biochem. Biophys. Res. Commun.* **226,** 672–680
12. Permanne, B., Adessi, C., Saborio, G. P., Fraga, S., Frossard, M. J., Van Dorpe, J., Dewachter, I., Banks, W. A., Van Leuven, F., and Soto, C. (2002) Reduction of amyloid load and cerebral damage in a transgenic mouse model of Alzheimer's disease by treatment with a β-sheet breaker peptide. *FASEB J.* **16,** 860–862
13. Soto, C., Sigurdsson, E. M., Morelli, L., Kumar, R. A., Castaño, E. M., and Frangione, B. (1998) β-Sheet breaker peptides inhibit fibrillogenesis in a rat brain model of amyloidosis. Implications for Alzheimer's therapy. *Nat. Med.* **4,** 822–826
14. Giordano, C., Masi, A., Pizzini, A., Sansone, A., Consalvi, V., Chiaraluce, R., and Lucente, G. (2009) Synthesis and activity of fibrillogenesis peptide inhibitors related to the 17–21 β-amyloid sequence. *Eur. J. Med. Chem.* **44,** 179–189
15. Giordano, C., Sansone, A., Masi, A., Masci, A., Mosca, L., Chiaraluce, R., Pasquo, A., and Consalvi, V. (2012) Inhibition of amyloid peptide fragment $A\beta_{25-35}$ fibrillogenesis and toxicity by N-terminal β-amino acid-containing esapeptides. Is taurine moiety essential for *in vivo* effects? *Chem. Biol. Drug. Des.* **79,** 30–37
16. Allen, M., and Tildesley, D. (1987) *Computer Simulations of Liquids,* Clarendon Press, Oxford
17. Hohenberg, P., and Kohn, W. (1964) Inhomogeneous electron gas. *Phys. Rev.* **136,** 864–871
18. Kohn, W., and Sham, L. J. (1965) Self-consistent equations including exchange and correlation effects. *Phys. Rev.* **140,** 1133–1138
19. Car, R., and Parrinello, M. (1985) Unified approach for molecular dynamics and density-functional theory. *Phys. Rev. Lett.* **55,** 2471–2474
20. Giannozzi, P., Jansen, K., La Penna, G., Minicozzi, V., Morante, S., Rossi, G., and Stellato, F. (2012) Zn induced structural aggregation patterns of β-amyloid peptides by first-principle simulations and XAS measurements. *Metallomics* **4,** 156–165
21. Miller, Y., Ma, B., and Nussinov, R. (2010) Zinc ions promote Alzheimer Aβ aggregation via population shift of polymorphic states. *Proc. Natl. Acad. Sci. U.S.A.* **107,** 9490–9495
22. Novick, P. A., Lopes, D. H., Branson, K. M., Esteras-Chopo, A., Graef, I. A., Bitan, G., and Pande, V. S. (2012) Design of β-amyloid aggregation inhibitors from a predicted structural motif. *J. Med. Chem.* **55,** 3002–3010
23. Crescenzi, O., Tomaselli, S., Guerrini, R., Salvadori, S., D'Ursi, A. M., Temussi, P. A., and Picone, D. (2002) Solution structure of the Alzheimer's disease Amyloid β peptide(1–42). *Eur. J. Biochem.* **269,** 5642–5648
24. Berendsen, H. J. C., van der Spoel, D., and van Drunen, R. (1995) GROMACS. A message-passing parallel molecular dynamics implementation. *Comp. Phys. Comm.* **91,** 43–56
25. Lindahl, E., Hess, B., and van der Spoel, D. (2001) GROMACS 3.0. A package for molecular simulation and trajectory analysis. *J. Mol. Model.* **7,** 306–317
26. Van Der Spoel, D., Lindahl, E., Hess, B., Groenhof, G., Mark, A. E., and Berendsen, H. J. (2005) GROMACS. Fast, flexible, and free. *J. Comput. Chem.* **26,** 1701–1718
27. Hess, B., Kutzner, C., van der Spoel, D., and Lindahl, E. (2008) GROMACS 4. Algorithms for highly efficient, load-balanced, and scalable molecular simulation. *J. Chem. Theory Comput.* **4,** 435–447
28. Oostenbrink, C., Villa, A., Mark, A. E., and van Gunsteren, W. F. (2004) A biomolecular force field based on the free enthalpy of hydration and solvation. The GROMOS force-field parameter sets 53A5 and 53A6. *J. Comput. Chem.* **25,** 1656–1676
29. Malde, A. K., Zuo, L., Breeze, M., Stroet, M., Poger, D., Nair, P. C., Oostenbrink, C., and Mark, A. E. (2011) An automated force field topology builder (ATB) and repository. Version 1.0. *J. Chem. Theo. Comp.* **7,** 4026–4037
30. Bussi, G., Donadio, D., and Parrinello, M. (2007) Canonical sampling through velocity rescaling. *J. Chem. Phys.* **126,** 014101
31. Berendsen, H. J. C., Postma, J. P. M., DiNola, A., and Haak, J. R. (1984) Molecular dynamics with coupling to an external bath. *J. Chem. Phys.* **81,** 3684–3690
32. Darden, T., York, D., and Pedersen, L. (1993) Particle mesh Ewald. An Nlog(N) method for Ewald sums in large systems. *J. Chem. Phys.* **98,** 10089–10092
33. Atherton, E., and Sheppard, R. (1989) *Solid Phase Synthesis. A Practical Approach.* IRL Press, Oxford
34. Brouwer, A. J., Monnee, M. C. F., and Liskamp, R. M. J. (2000) An efficient synthesis of *N*-protected β-aminoethanesulfonyl chlorides. Versatile building blocks for the synthesis of oligopeptidosulfonamides. *Synthesis* **11,** 1579–1584
35. Naiki, H., Higuchi, K., Hosokawa, M., and Takeda, T. (1989) Fluorometric determination of amyloid fibrils *in vitro* using the fluorescent dye thioflavine T. *Anal. Biochem.* **177,** 244–249
36. Henry, E. R., and Hofrichter, J. (1992) Singular value decomposition. application to analysis of experimental data. *Methods Enzymol.* **210,** 129–192
37. Johnson, W. C., Jr. (1992) Analysis of circular dichroism spectra. *Methods Enzymol.* **210,** 426–447
38. Ionescu, R. M., Smith, V. F., O'Neill, J. C. Jr., and Matthews, C. R. (2000) Multistate equilibrium unfolding of *Escherichia coli* dihydrofolatereductase. Thermodynamic and spectroscopic description of the native, intermediate, and unfolded ensembles. *Biochemistry* **39,** 9540–9550
39. Maiorov, V. N., and Crippen, G. M. (1995) Size-independent comparison of protein three-dimensional structures. *Proteins* **22,** 273–283
40. Lemkul, J. A., and Bevan, D. R. (2012) The role of molecular simulations in the development of inhibitors of amyloid β-peptide aggregation for the treatment of Alzheimer's disease. *ACS Chem. Neurosci.* **3,** 845–856
41. Kabsch, W., and Sander, C. (1983) Dictionary of protein secondary structure. Pattern recognition of hydrogen-bonded and geometrical features. *Biopolymers* **22,** 2577–2637
42. Ito, M., Johansson, J., Strömberg, R., and Nilsson, L. (2011) Unfolding of the amyloid β-peptide central helix. Mechanistic insights from molecular dynamics simulations. *PLoS ONE* **6,** e17587
43. Ito, M., Johansson, J., Strömberg, R., and Nilsson, L. (2012) Effects of ligands on unfolding of the amyloid β-peptide central helix. Mechanistic insights from molecular dynamics simulations. *PLoS ONE* **7,** e30510
44. Bartolini, M., Bertucci, C., Bolognesi, M. L., Cavalli, A., Melchiorre, C., and Andrisano, V. (2007) Insight into the kinetic of amyloid β (1–42) peptide self-aggregation. Elucidation of inhibitors' mechanism of action. *Chembiochem* **8,** 2152–2161
45. Necula, M., Kayed, R., Milton, S., and Glabe, C. G. (2007) Small molecule inhibitors of aggregation indicate that amyloid β oligomerization and fibrillization pathways are independent and distinct. *J. Biol. Chem.* **282,** 10311–10324
46. Woody, R. W., and Dunker, A. K. (1996) *in Circular Dichroism and the Conformational Analysis of Biomolecules.* Plenum Press, New York
47. Laczkó, I., Vass, E., Soós, K., Fülöp, L., Zarándi, M., and Penke, B. (2008) Aggregation of Aβ(1–42) in the presence of short peptides. Conformational studies. *J. Pept. Sci.* **14,** 731–741
48. Loo, J. A. (2000) Electrospray ionization mass spectrometry. A technology for studying noncovalent macromolecular complexes. *Int. J. Mass Spectrom.* **200,** 175–186
49. Bazoti, F. N., Tsarbopoulos, A., Markides, K. E., and Bergquist, J. (2005) Study of the non-covalent interaction between amyloid-β-peptide and melatonin using electrospray ionization mass spectrometry. *J. Mass Spectrom.* **40,** 182–192